

# Observation of trap-assisted formation of atom-ion bound states

Meirav Pinkas, Or Katz,\* Jonathan Wengrowicz, Nitzan Akerman, and Roei Ozeri  
*Department of Physics of Complex Systems and AMOS,  
 Weizmann Institute of Science, Rehovot 7610001, Israel*

Pairs of free particles cannot form bound states in elastic collision due to momentum and energy conservation. In many ultracold experiments, however, the particles collide in the presence of an external trapping potential which can couple the center-of-mass and relative motions and assist the formation of bound-states. Here, we report on observation of weakly bound molecular states formed between one ultracold  $^{87}\text{Rb}$  atom and a single trapped  $^{88}\text{Sr}^+$  ion in the presence of a linear Paul trap. We show that bound states can form efficiently in binary collisions, and enhance the rate of inelastic processes. By observing electronic spin-exchange rate, we study the dependence of these bound states on the collision energy and magnetic field and extract the average molecular binding energy  $E_{\text{bind}} = 0.7(1) \text{ mK} \cdot k_B$  and the mean lifetime of the molecule  $\tau = 0.3(1) \mu\text{s}$ , with good agreement with molecular-dynamics simulations. Our simulations predict a highly unusual power-law distribution of molecular lifetimes with a mean that is dominated by extreme, long-lived, events. The dependence of the molecular properties on the trapping parameters opens new avenues to study and control ultracold collisions.

## INTRODUCTION

Collisions between pairs of particles are among the fundamental building blocks of molecular formation and quantum chemistry. Owing to energy and momentum conservation, pairs of free particles cannot bind in binary elastic collisions; instead, formation of molecules usually requires inelastic dynamics or three-body interactions, as realized in processes such as photo-association [1–4], Feshbach-association [5–9] or three body recombination [10–12].

In many ultracold collision experiments, however, the particles are not free but rather trapped by an external potential, as optical-dipole traps [13–17] or ion traps [9, 11, 18–23]. Charged particles, in particular, are highly susceptible to electric fields and usually require strong electromagnetic potentials to assist the trapping. In most trapped ion experiments, the ions are held in a Paul trap, using time-dependent electric fields [24, 25].

Various works have shown that the presence of a trap can modify the properties of collisions and lead to emergence of unique phases [26, 27], to change in the profile of scattering resonances [27–31], to non-equilibrium dynamics [32, 33] or to formation of bound states via adiabatic merge of two different traps [34–37]. Yet, to date, trapped assisted bound states between pairs of neutral atoms and atomic ions have not been observed.

Here we show that the confinement of the ion can lead to formation of a short-lived and loosely bound  $^{88}\text{Sr}^+ - ^{87}\text{Rb}$  molecule in a cold binary collision. By measuring the probability of electronic spin-exchange (SE) between the atom and ion at different settings, we estimate the molecule’s lifetime and the binding energy. We compare

our results to a numerical simulation and characterize the effect of the trap for various experimental configurations. We show that the lifetime of these molecules is power-law distributed such that the mean molecular lifetime is dominated by extreme, long-lived, events.

## FORMATION AND DETECTION OF ATOM-ION BOUND STATES

In most hybrid atom-ion experiments in the ultracold regime, both neutral atom and ion are trapped by external potentials. Yet, the dynamics is predominantly governed by the ion’s trapping potential owing to its considerably larger depth. This potential breaks the translation invariance symmetry of the interaction Hamiltonian and could hence generate coupling between the relative motion and the center-of-mass motion of the atom-ion pair. This coupling could transfer energy between these two frames and reduce the pair’s energy in the relative frame, and by that allow for formation of short-lived bound states. A similar mechanism leads to a creation of a bound state of ultracold atoms in an anharmonic trap [38, 39] or when the particles have different trapping frequencies [40].

We illustrate the formation of a bound state in Fig. 1a, via numerical simulation of a collision in the presence of an ideal, spherical symmetric harmonic potential that applies trapping forces only on the ion (see Methods). Here the atom and ion bind in a binary collision; Their relative motion manifests multiple oscillations, shown in the center-of-mass frame. Consequently, during the lifetime of this molecule, the pair comes into close contact multiple times and by that enhances the action of short-range chemical forces during the scattering, which could effect the probability of inelastic processes.

---

\* Present address: Department of Electrical and Computer Engineering, Duke University, Durham, North Carolina 27708, USA

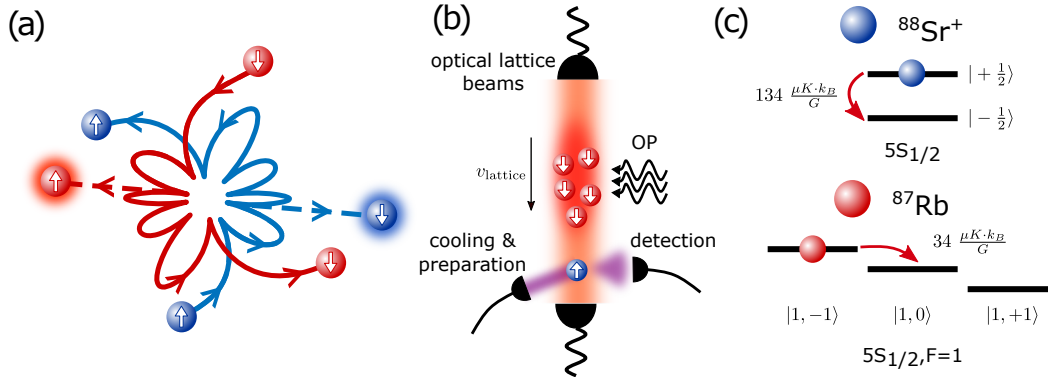


Figure 1. **Bound state formation and experimental apparatus.** (a) A collision between an atom and an ion in center of mass frame when the ion is trapped in an harmonic trap. A bound state with five short-range collisions is formed (solid lines). If an exothermic spin exchange occurs, shown here schematically in the second collision, the energy is released and the bound state may dissociate (dashed lines). (b) The experimental setup. A cloud of Rb atoms is trapped, cooled down, and loaded into an optical lattice trap. The atoms are optically pumped (OP) into a specific spin state. The atomic cloud is transported over the ion at a velocity  $v_{\text{lattice}}$ . The ion is prepared in a specific spin state prior to the passage of the cloud, and typically a single Langevin collision occur. Detection of the ion state is realized afterwards using state-selective fluorescence. (c) Energy levels for  $^{88}\text{Sr}^+$  and  $^{87}\text{Rb}$  in the electronic ground state. After a spin-exchange process, denoted by the red arrows, the Zeeman energy is released or absorbed to the motional degrees of freedom.

The total inelastic scattering probability of an ion inside a cloud of neutral atoms depends on the number of scattering events with different atoms and on the probability outcome of a scattering by one atom. The number of distinct scattering events with different atoms is determined by the Langevin capture rate coefficient  $K_L$ , which depends on the mass of the atoms and the neutral atom polarizability [3]. In each Langevin collision, the atom and ion spiral towards each other, and have a single period of interaction if they remain free or multiple periods of short range interactions if a bound state is formed. At each short-range passage, an inelastic process can occur with some probability that is determined by the molecular potentials curves at short range [3, 41]. Owing to the longer characteristic mechanical length of the trap with respect to the range of chemical forces, to a good approximation, the formation of a weakly bound state manifests as an increase in the number of short-range passages, which does not alter the inelastic probability by a single passage. Therefore, the enhancement of the inelastic probability can serve as a probe to detect and characterize atom-ion bound states.

## EXPERIMENTAL SYSTEM

We study the formation of loosely bound  $^{87}\text{Rb}$ - $^{88}\text{Sr}^+$  molecules using the experimental system that is shown in Fig. 1b and detailed in Refs. [33, 42, 43]. In brief, we trap and cool  $^{87}\text{Rb}$  atoms in a magneto-optical trap (MOT) with a dark-MOT stage followed by a polarization gradient cooling. A cloud of  $(5 - 10) \times 10^5$

atoms is loaded into a 1D optical lattice created by two counter-propagating Nd:YAG laser beams [43]. The atoms are optically pumped into one of the hyperfine states  $|F = 1, m_F = \pm 1\rangle$  in the electronic ground-state. The atomic cloud is transported through the Paul trap at a fixed velocity of 0.14 mm/ms, which is controlled by the relative frequency difference between the optical lattice beams. A  $^{88}\text{Sr}^+$  ion is trapped in a linear segmented Paul trap and is cooled using Doppler cooling, followed by resolved-sideband cooling into the ground state ( $\bar{n} \lesssim 0.5$  quanta for each of the motional modes). Then, the ion is optically pumped into one of the two Zeeman states of the electronic ground-state manifold  $5S_{1/2}$ . Following preparation, and before overlapping with the atomic cloud, the magnetic field is changed from 3 G to a target value between 0.5 and 20 G using a pair of Helmholtz coils. Excess-micromotion (EMM) is compensated every hour during the experiment to less than  $50 \mu\text{K}$  for each of the radial modes and to a few  $\mu\text{K}$  in the axial direction.

After the atomic cloud passes the ion, the magnetic field is ramped back to its initial value for state-detection of the ion. Due to the long relaxation time of the magnetic field in the system, the detection takes place 70 ms after the current in the quantization coils returns to its initial value. We measure the spin state of the ion by double-shelving of one of the ground state levels into two different Zeeman states in the  $4D_{5/2}$  manifolds using a narrow linewidth laser at 674nm, followed by detection of state-dependent fluorescence light using the strong  $5S_{1/2}$ - $5P_{1/2}$  dipole transition.

## ENHANCEMENT OF SPIN-EXCHANGE RATE

Spin-exchange is one of the most probable inelastic processes that occurs in collisions of  $^{88}\text{Sr}^+$  and  $^{87}\text{Rb}$  [41, 44], which can be enhanced by the formation of molecules. In Fig. 1(c) we illustrate a spin exchange processes between  $^{88}\text{Sr}^+$  and  $^{87}\text{Rb}$  in its lower hyperfine manifold. In the presence of a magnetic field, the exchange of spin is accompanied by exchange of internal magnetic energy and kinetic energy. We studied the exothermic channel via measurement of spin flip of the ion when the pair is prepared in the initial state  $|\uparrow\rangle_{\text{Sr}^+} |1, -1\rangle_{\text{Rb}}$ , and also the endothermic channel when the initial state is  $|\downarrow\rangle_{\text{Sr}^+} |1, +1\rangle_{\text{Rb}}$ . An example for an exothermic transition is shown schematically in Fig. 1(c). The energy gap for these two pathways depends on the magnetic field and equal to  $\Delta_{\text{SE}} = \pm h \cdot 3.5 \frac{\text{MHz}}{\text{G}} = \pm 168 \frac{\mu\text{K} \cdot k_B}{\text{G}}$ , where  $h$  is Planck's constant and  $k_B$  is Boltzmann's constant.

In the experiment, the mean number of Langevin capturing events per passage of the atomic cloud through the ion trap is nearly independent of the energy or magnetic field, and is given by  $N_L = \rho K_L / v_{\text{lattice}}$ , where  $\rho$  is the atomic column density integrated along the lattice direction of motion, and  $v_{\text{lattice}}$  is the lattice velocity. The probability to multiple different Langevin events in a single passage of the cloud is small. The Langevin calibration process is described in Ref. [45] and in the Methods section.

### A. Energy dependence

We first study the dependence of spin-exchange on the ions' excess micromotion (EMM) energy  $E_{\text{EMM}}$ , which is the energy in the fast oscillatory motion in the frequency of the trapping rf fields.  $E_{\text{EMM}}$  is determined by the voltage  $\Delta V_{\text{comp}}$  applied on one of the trap electrode. In Fig. 2 we show the dependence of the measured spin-exchange probability per passage,  $p_{\text{SE}}^{\text{pass}}$ , of the cloud on the micromotion energy at a background field of  $B = 16$  G.

While in the absence of a bound state we expect  $p_{\text{SE}}^{\text{pass}}$  to be independent of the micromotion energy, our measurement shows enhancement of the exothermic channel at small  $E_{\text{EMM}}$ . The measured ratio of spin-exchange probability and the probability of a Langevin collision varies between  $\sim 10\%$  at high EMM to  $\sim 30\%$  at low EMM. The enhancement of SE probability at low micromotion energies is an indication of the formation of a bound state, which leads to multiple short-range collisions.

For the endothermic channel, spin-exchange probability is slightly suppressed at low micromotion energies. The exchange probability of the endothermic channel should be suppressed with respect to the exothermic

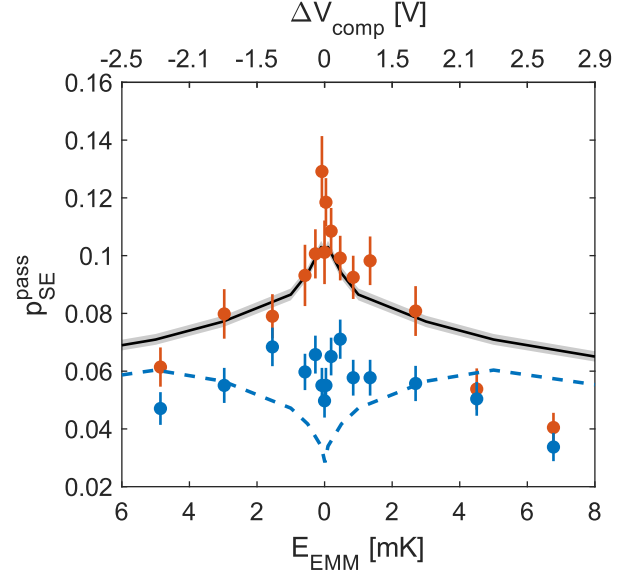


Figure 2. **Spin-exchange as a function of collision energy.** Spin exchange probability per passage as function of excess-micromotion energy is measured at 16 G for exothermic (red) and endothermic (blue) channels. Error bars are binomial distribution standard deviation. Black solid line is a maximum likelihood fit to the short-range spin-exchange probability based on a numerical simulation (see main text for details), giving a probability of  $p_{\text{SE}}^0 = 0.101(3)$ . Shaded area is  $1\sigma$  confidence bounds of the fit. Dashed blue line is the effective spin-exchange given by the simulation for the endothermic at  $B=16$  G transition when the short-range probability is 0.1.

one, if the kinetic energy of the bodies or the work done by the trap is smaller than the magnetic energy gap. At 16 G, the energy gap for an endothermic transition is about 2.5 mK, well above the collision energy at low EMM values. The lack of complete suppression of endothermic spin-exchange is another indication of trap associated effects, that could be explained by multiple short-range collisions during which work can be done by the trap time-dependent fields.

### B. Magnetic field dependence

We next turned to measuring spin-exchange dynamics at various magnetic fields. Owing to the conversion between internal magnetic energy and kinetic energy, we expect to see enhancement or suppression of spin-exchange as a function of the magnetic field for different scattering pathways if a bound state is formed. The measured endothermic (exothermic) spin-exchange probability as a function of the magnetic field is shown by the blue (red) filled-circles in Fig. 3.

The enhancement of the exothermic channel can be

understood by the fact that, the Zeeman energy will be released into the motional degrees of freedom. In cases where the Zeeman energy is larger than the binding energy, the molecule will dissociate following spin-exchange, and no further spin-exchange that reverse the spin state can occur. But, whenever this energy is lower than the binding energy of the molecule, multiple spin-exchange events can happen. Even number of spin-exchange events will leave the ion in its initial spin state but odd number of events would result in a spin flip and to reduction of the spin-exchange probability compared to high values of the magnetic field. By this assumption, we then expect that for a large number of short-range collisions within the molecular lifetime the spin-exchange rate will saturate at the Langevin rate at high magnetic fields and to half the Langevin rate at low fields.

For the endothermic channel, spin-exchange still occurs in the highest measured magnetic field of 20 G, despite the fact it corresponds to an energy gap of above 3 mK, which is larger than all other initial energy scales in the system. We further characterized the dynamics by measuring the temperature of the ion, post-selected on experiments in which its spin had flipped. The measured temperatures are shown in Fig. 3(b-c), using the Rabi carrier thermometry technique [21]. A reference temperature of non spin-exchange events was measured separately for each channel (see methods). At a magnetic field of 3 G, both exothermic (red) and endothermic (blue) pathways leave the ion at a similar temperature, of about 1 mK, which is likely dominated by heating driven by the fields of the Paul trap [21, 46]. At the highest magnetic field of 20 G, after an exothermic transition, the ion heats up to a temperature comparable with the Zeeman gap, of about 4 mK. Surprisingly, after an endothermic transition, the temperature of the ion is similar to that measured at the low magnetic field, without any observed reduction of the kinetic energy, which is expected because of the Zeeman energy barrier. This might indicate additional trap-induced effects in this regime.

## MOLECULAR DYNAMICS SIMULATIONS

We compared our observations to a molecular-dynamics (MD) model, numerically simulating the dynamics of the collisions in a Paul trap (see Methods). Using the simulation, we can study the distribution of number short-range collisions,  $N$ . We find that for our experimental trapping parameters, a bound state is typically formed in a Langevin collision when excess micromotion is compensated ( $E_{\text{EMM}} = 0$ ), as can be seen as blue line in Fig. 4(a). In addition, the tail of the distribution exhibits a power-law behavior, which scales roughly as  $1/N^2$ . For this power-law distribution, the

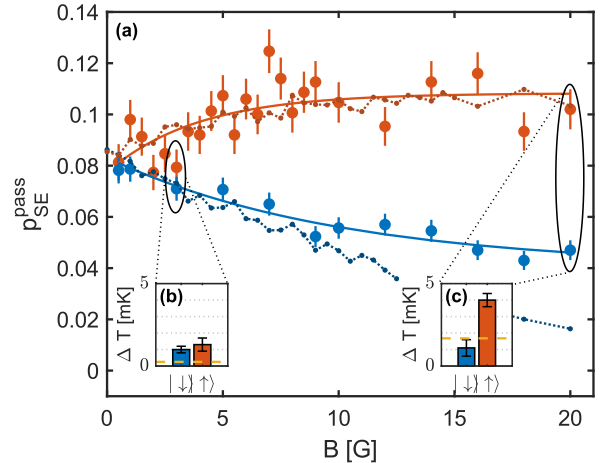


Figure 3. **Spin-exchange as a function of the magnetic field and thermometry.** (a) Spin-exchange probability per passage as a function of the magnetic field for the exothermic (red) and endothermic (blue) channels at lattice velocity 0.14 mm/ms (equivalent to 100  $\mu$ K). Error bars are binomial distribution standard deviation. Solid lines are maximum-likelihood estimation fit to a decay exponential function  $p_{\text{SE}}^{\text{pass}} = A \cdot \exp(-B/B_0) + C$  for both experiments. The parameters are,  $A=-0.031(4)$ ,  $B_0=3.9(7)$  G and  $C=0.108(2)$  for the exothermic channel, and  $A=0.043(3)$ ,  $B_0=10(1)$  G and  $C=0.040(1)$  for the endothermic channel. Dotted lines are expected  $p_{\text{SE}}^{\text{pass}}$  for the exothermic (red) and endothermic channels (blue) from the MD simulation, assuming the short-range  $p_{\text{SE}}^0 = 0.101(3)$  that was found using the data in Fig. 3. (b) Heating of the ion using Rabi carrier thermometry on the spin-exchange event of the two transitions at 3 G (b) and 20 G (c). The dashed yellow line denotes the energy of half of the Zeeman gap.

mean number of short-range collisions, and therefore the mean molecular lifetime, is dominated by rare tail events.

When the collision energy is increased, the probability for more than one short-range collision,  $p_{\text{bound}}$ , is reduced, as can be seen in Fig. 4(b). This coincides with the observed reduced spin-exchange probability at larger EMM in Fig. 2. However, bound states still occur with high probability up to 10 mK. When the collision occurs with high EMM, the collision energy depends on the momentary phase of the rf field, and therefore low energy events are still possible. In addition, the power-law tail of the distribution is suppressed at higher values of micromotion, e.g. at  $E_{\text{EMM}} = 10$  mK (red line in Fig. 4(a)).

From the simulation we extracted the numerical probability distribution function (PDF) of the number of short-range collisions,  $N$ , for each micromotion energy. We then calculated the effective spin-exchange probability per a single passage for the high magnetic field exothermic process (see methods). Then, by a max-

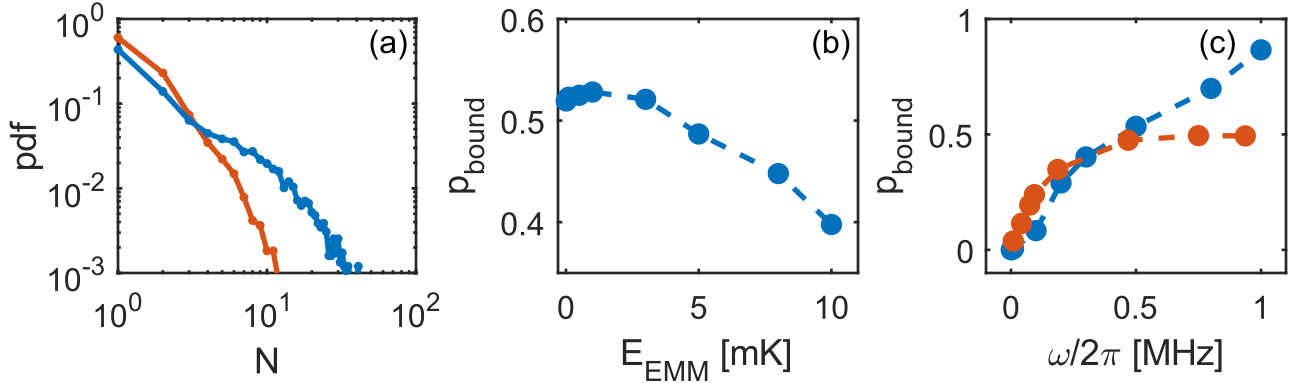


Figure 4. **Bound state properties from a molecular dynamics simulation.** (a) Probability density function (pdf) of the number of short-range collisions between  $\text{Sr}^+$ -Rb pair when the EMM is compensated (blue), and equivalent to 10 mK (red). (b) Bound states fraction, out of the Langevin collisions, as a function of EMM energy (c) Bound states fraction in a harmonic trap (blue) and a Paul trap (red) as function of trap frequency. The harmonic trap is a spherical symmetric trap with a frequency  $\omega$ . The Paul trap is a linear trap with an axial frequency  $\omega_{ax} = 2\pi \cdot 3$  kHz, radial frequency  $\omega$  and rf frequency  $\Omega_{rf} = 2\pi \cdot 26.51$  MHz, for an ion with zero initial energy. In all simulations the Rb atoms have a velocity equivalent to  $100\mu\text{K}$ . Confidence bounds are smaller than markers size.

imum likelihood estimation to the measured data, we determined the microscopic spin-exchange probability per one period of short-range interaction in the exothermic channel of  $p_{\text{SE}}^0 = 0.101(3)$ . This estimation of microscopic spin-exchange rate is consistent with previous measurements [47]. The prediction of our numerical simulation for  $p_{\text{SE}}^{\text{pass}}$  vs.  $E_{\text{EMM}}$  using this fitted value is shown in Fig. 2 by the black solid line with grey confidence interval around it and is in good agreement with our measured data. The dashed blue line shows the predictions of our model for the endothermic channel. As seen, our model predicts a much stronger suppression of  $p_{\text{SE}}^{\text{pass}}$  at low  $E_{\text{EMM}}$  than we measure.

Using the estimated microscopic spin-exchange probability, we can further simulate the dynamics of the spin-exchange processes for different magnetic fields. We present the expected  $p_{\text{SE}}^{\text{pass}}$  of the numerical molecular-dynamics simulation in dotted lines in Fig. 3 with the same microscopic spin-exchange probability,  $p_{\text{SE}}^0$ , and no fit parameters. The simulation results are in good agreement with the enhancement of exothermic spin-exchange as function of the magnetic field, and the suppression of the endothermic spin-exchange in the low magnetic field regime. Again, at a high magnetic field, the observed endothermic spin-exchange is higher than predicted by our model. This might indicate additional trap-induced effects or an enhancement of the spin-exchange cross-section for the endothermic channel at high magnetic fields.

The formation of trapped-induced bound states is a universal phenomena that can emerge at different trap configurations. For example, in Fig. 4(c) we show the probability for more than one short-range collision,

$p_{\text{bound}}$ , as a function of the trap secular frequency  $\omega$ . Here both for an an ideal, time-independent spherical symmetric harmonic trap (blue) and a Paul trap with radial frequency  $\omega$  and fixed axial frequency of 3 kHz. As seen in the figure, the presence of both traps leads to the formation of bound states in binary collisions. For the harmonic case the probability to form a bound-state increases with the trap frequency to close to unity, but saturates for a Paul trap at  $p_{\text{bound}} \simeq 0.5$ , owing to work done by the time-dependent fields that heats the ion up and prevents molecular binding [46]. These results highlight that the formation of bound-state is predominantly associated with the breaking of translation symmetry and not on the presence of time-dependent fields and energy non-conservation of atom-ion collisions in Paul traps.

## BINDING ENERGY AND LIFETIME OF TRAPPED-ASSISTED BOUND STATES

We can use our measured data to estimate different parameters of the loosely bound molecules. A maximum likelihood estimation of the magnetic dependence of the exothermic channel to an exponential decay gives a decay constant of  $B_0 = 3.9(7)$  G, which corresponds to mean bond energy of  $E_{\text{bind}} = \Delta_{\text{SE}} B_0 = 0.7(1)$  mK. The likelihood of the exponential decay can be compared to a constant probability model using a likelihood ratio test, giving a p-value of  $1.2 \cdot 10^{-5}$ .

The number of short-range collisions and the resulting molecular lifetime can be estimated directly from the experiment by its effect on the probability of spin-

exchange in a single pass of the atomic cloud. The bound state can be modeled by assuming that the number of short-range interaction periods,  $N$ , has a geometric distribution with a probability  $1/\langle N \rangle$  and the probability of a spin-exchange event is constant,  $p_{SE}^0$ . Then, the observed spin-exchange probability can be calculated in low and high magnetic fields for  $p_{SE}^0 = 0.101$ . The calculated value can be compared to the measured value, giving  $\langle N \rangle = 10(3)$  (see methods). Taking the long-range asymptotic of the polarization potential between the pair and the binding energy, we can estimate the maximal distance between the particles  $r_{max} = 27$  nm. The falling time of two free particles can be calculated analytically and is given by  $t = \sqrt{\frac{\mu}{9C_4}} r_{max}^3$  [46], which gives a falling time of  $t = 17$  ns. Therefore, the period of oscillation is  $T = 34$  ns and we can estimate the lifetime of the molecule in the experiment by  $0.3(1)$   $\mu$ s. This coincides with the mean lifetime of the molecule in the simulation, which is  $0.411(4)$   $\mu$ s.

## DISCUSSION

We have observed the formation of trap-assisted bound state in ultra-cold atom-ion collisions. These bound states amplify the rate of inelastic processes in both the exothermic and endothermic collision channels. From the measurements of the spin-exchange rates, we estimated the average binding energy of these molecules by  $0.7(1)$  mK and the molecule mean lifetime by  $0.3(1)$   $\mu$ s.

Remarkably, bound states are efficiently formed in binary collisions. Numerical simulations indicate formation every other collisions, and molecular life-time with a power-law distribution; a highly unusual behavior. Power-law in the energy distribution were already observed in atom-ion collisions due to multiplicative energy fluctuations after multiple collisions [21, 32, 33].

However, in this case, the power-law arises in a single collision.

The molecular binding probability and lifetime can be controlled by the trap parameters which can serve as a convenient control knob. Since the coupling between the relative motion and center-of-mass motion depends on the reduced mass, this effect will probably be suppressed for a lower reduced mass [48].

We observe that trap-assisted bound states are formed also, and even more efficiently, in static potentials. This indicates that the source for binding is the coupling between relative and center-of-mass motion by the breaking of translational symmetry rather than the presence of time-dependent fields in Paul traps. This effect can also play a role in atom-ion interactions using an optical trap for the ions [15]. In addition, since this is a predominantly low-energy effect, it can potentially have consequences on observations near the s-wave limit [9, 48].

Here we have explained our observations using classical simulations and did not include any quantum effects. However the effects of the magnetic field and collision energy on “sticky collisions” [49] and molecular formation could be related, in a quantum description to wavefunction resonances. Moreover, we see a significant deviation of our measured spin-exchange cross section in the endothermic channel, at low energy and strong magnetic field, from the predictions of our simulations. This could be due to the effect of multiple overlapping Feshbach resonances at these magnetic fields.

## ACKNOWLEDGMENTS

This work was supported by the Israeli Science Foundation and the Goldring Family Foundation.

- 
- [1] K. M. Jones, E. Tiesinga, P. D. Lett, and P. S. Julienne. Ultracold photoassociation spectroscopy: Long-range molecules and atomic scattering. *Rev. Mod. Phys.*, 78(2):483–535, 2006.
  - [2] Z. Idziaszek, A. Simoni, T. Calarco, and P. S. Julienne. Multichannel quantum-defect theory for ultracold atom-ion collisions. *New Journal of Physics*, 13(8):083005, 2011.
  - [3] M. Tomza, K. Jachymski, R. Gerritsma, A. Negretti, T. Calarco, Z. Idziaszek, and P. S. Julienne. Cold hybrid ion-atom systems. *Reviews of modern physics*, 91(3):035001, 2019.
  - [4] S. Jyothi, T. Ray, S. Dutta, A. Allouche, R. Vexiau, O. Dulieu, and SA Rangwala. Photodissociation of trapped  $Rb_2^+$ : Implications for simultaneous trapping of atoms and molecular ions. *Physical review letters*, 117(21):213002, 2016.
  - [5] T. Köhler, K. Góral, and P. S. Julienne. Production of cold molecules via magnetically tunable Feshbach resonances. *Reviews of Modern Physics*, 78(4):1311–1361, 2006.
  - [6] C. Chin, R. Grimm, P. Julienne, and E. Tiesinga. Feshbach resonances in ultracold gases. *Rev. Mod. Phys.*, 82(2):1225–1286, 2010.
  - [7] H. Hirzler, R.S. Lous, E. Trimby, J. Pérez-Ríos, A. Safavi-Naini, and R. Gerritsma. Observation of chemical reactions between a trapped ion and ultracold feshbach dimers. *Physical Review Letters*, 128(10):103401, 2022.
  - [8] B. Drews, M. Deiß, K. Jachymski, Z. Idziaszek, and



- J. Hecker Denschlag. Inelastic collisions of ultracold triplet  $\text{Rb}_2$  molecules in the rovibrational ground state. *Nature communications*, 8(1):1–7, 2017.
- [9] P. Weckesser, F. Thielemann, D. Wiater, A. Wojciechowska, L. Karpa, K. Jachymski, M. Tomza, T. Walker, and T. Schaetz. Observation of feshbach resonances between a single ion and ultracold atoms. *Nature*, 600(7889):429–433, 2021.
- [10] A. Härter, A. Krüchow, A. Brunner, W. Schnitzler, S. Schmid, and J. H. Denschlag. Single ion as a three-body reaction center in an ultracold atomic gas. *Physical review letters*, 109(12):123201, 2012.
- [11] A. Mohammadi, A. Krüchow, A. Mahdian, M. Deiß, J. Pérez-Ríos, H. da Silva Jr, M. Raoult, O. Dulieu, and J. H. Denschlag. Life and death of a cold  $\text{BaRb}^+$  molecule inside an ultracold cloud of rb atoms. *Physical Review Research*, 3(1):013196, 2021.
- [12] A. Krüchow, A. Mohammadi, A. Härter, J. H. Denschlag, J. Pérez-Ríos, and C. H. Greene. Energy scaling of cold atom-atom-ion three-body recombination. *Physical Review Letters*, 116(19):193201, 2016.
- [13] R. Grimm, M. Weidemuller, and Y. B. Ovchinnikov. *Optical Dipole Traps*, volume 42. 2000.
- [14] L. Anderegg, L. W. Cheuk, Y. Bao, S. Burchesky, W. Ketterle, K.K. Ni, and J. M. Doyle. An optical tweezer array of ultracold molecules. *Science*, 365:1156–1158, 2019.
- [15] A. Lambrecht, J. Schmidt, P. Weckesser, M. Debatin, L. Karpa, and T. Schaetz. Long lifetimes and effective isolation of ions in optical and electrostatic traps. *Nature Photonics*, 11:704–707, 2017.
- [16] L. A. Reynolds, E. Schwartz, U. Ebling, M. Weyland, J. Brand, and M. F. Andersen. Direct Measurements of Collisional Dynamics in Cold Atom Triads. *Physical Review Letters*, 124(7):73401, 2020.
- [17] J. Schmidt, P. Weckesser, F. Thielemann, T. Schaetz, and L. Karpa. Optical traps for sympathetic cooling of ions with ultracold neutral atoms. *Physical review letters*, 124(5):053402, 2020.
- [18] A. T. Grier, M. Cetina, F. Oručević, and V. Vuletić. Observation of cold collisions between trapped ions and trapped atoms. *Physical Review Letters*, 102(22):1–4, 2009.
- [19] L. Ratschbacher, C. Zipkes, C. Sias, and M. Köhl. Controlling chemical reactions of a single particle. *Nature Physics*, 8:649–652, 2012.
- [20] F. H.J. Hall and S. Willitsch. Millikelvin reactive collisions between sympathetically cooled molecular ions and laser-cooled atoms in an ion-atom hybrid trap. *Physical Review Letters*, 109:3–7, 2012.
- [21] Z. Meir, T. Sikorsky, R. Ben-Shlomi, N. Akerman, Y. Dallal, and R. Ozeri. Dynamics of a Ground-State Cooled Ion Colliding with Ultracold Atoms. *Physical Review Letters*, 117(24):1–7, mar 2016.
- [22] R. Saito, S. Haze, M. Sasakawa, R. Nakai, M. Raoult, H. Da Silva, O. Dulieu, and T. Mukaiyama. Characterization of charge-exchange collisions between ultracold  $^6\text{Li}$  atoms and  $^{40}\text{Ca}^+$  ions. *Phys. Rev. A*, 95:032709, Mar 2017.
- [23] J. Joger, H. Furst, N. Ewald, T. Feldker, M. Tomza, and R. Gerritsma. Observation of collisions between cold Li atoms and  $\text{Yb}^+$  ions. *Physical Review A*, 96(3):1–6, 2017.
- [24] W. Paul. Electromagnetic Traps for Charged and Neutral Particles (Nobel Lecture). *Angewandte Chemie International Edition in English*, 29(7):739–748, 1990.
- [25] D. Leibfried, R. Blatt, C. Monroe, and D. Wineland. Quantum dynamics of single trapped ions. *Review of Modern Physics*, 75(1):281–324, 2003.
- [26] Z. Hadzibabic, P. Krüger, M. Cheneau, B. Battelier, and J. Dalibard. Berezinskii-Kosterlitz-Thouless crossover in a trapped atomic gas. *Nature*, 441(7097):1118–1121, 2006.
- [27] T. Kinoshita, T. Wenger, and D. S. Weiss. Observation of a One-Dimensional Tonks-Girardeau Gas. *Science*, 305(August):1125–1129, 2004.
- [28] M. Olshani. Atomic scattering in the presence of an external confinement and a gas of impenetrable bosons. *Physical Review Letters*, 81(5):938–941, 1998.
- [29] F. H. Mies, E. Tiesinga, and P. S. Julienne. Manipulation of Feshbach resonances in ultracold atomic collisions using time-dependent magnetic fields. *Physical Review A - Atomic, Molecular, and Optical Physics*, 61(2):17, 2000.
- [30] E. Haller, M. J. Mark, R. Hart, J. G. Danzl, L. Reichsöllner, V. Melezhik, P. Schmelcher, and H. C. Nägerl. Confinement-induced resonances in low-dimensional quantum systems. *Physical Review Letters*, 104(15):1–4, 2010.
- [31] J. P. Kestner and L. M. Duan. Anharmonicity-induced resonances for ultracold atoms and their detection. *New Journal of Physics*, 12, 2010.
- [32] I. Rouse and S. Willitsch. Superstatistical Energy Distributions of an Ion in an Ultracold Buffer Gas. *Physical Review Letters*, 118(14):1–6, 2017.
- [33] Z. Meir, M. Pinkas, T. Sikorsky, R. Ben-Shlomi, N. Akerman, and R. Ozeri. Direct Observation of Atom-Ion Nonequilibrium Sympathetic Cooling. *Physical Review Letters*, 121(5):53402, 2018.
- [34] R. Stock, H. D. Ivan, and E. L. Bolda. Quantum state control via trap-induced shape resonance in ultracold atomic collisions. *Physical Review Letters*, 91, 2003.
- [35] Z. Idziaszek, T. Calarco, and P. Zoller. Controlled collisions of a single atom and an ion guided by movable trapping potentials. *Physical Review A*, 76(3):033409, 2007.
- [36] V. S. Melezhik and A. Negretti. Confinement-induced resonances in ultracold atom-ion systems. *Physical Review A*, 94:1–8, 2016.
- [37] V. S. Melezhik, Z. Idziaszek, and A. Negretti. Impact of ion motion on atom-ion confinement-induced resonances in hybrid traps. *Physical Review A*, 100(6):063406, 2019.
- [38] S. Sala, P. I. Schneider, and A. Saenz. Inelastic confinement-induced resonances in low-dimensional quantum systems. *Physical Review Letters*, 109(7):1–5, 2012.
- [39] S. Sala, G. Zürn, T. Lompe, A. N. Wenz, S. Murmann, F. Serwane, S. Jochim, and A. Saenz. Coherent molecule formation in anharmonic potentials near confinement-induced resonances. *Physical Review Letters*, 110(20):1–5, 2013.
- [40] V. S. Melezhik and P. Schmelcher. Quantum dynamics of resonant molecule formation in waveguides. *New Journal of Physics*, 11:73031–73041, 2009.

- [41] R. Côté, a. Dalgarno, R Co, R. Côté, and a. Dalgarno. Ultracold atom-ion collisions. *Physical Review A*, 62(1):12709, 2000.
- [42] O. Katz, M. Pinkas, N. Akerman, and R. Ozeri. Quantum logic detection of collisions between single atom–ion pairs. *Nature Physics*, 2022.
- [43] R. Ben-shlomi, M. Pinkas, Z. Meir, T. Sikorsky, O. Katz, N. Akerman, and R. Ozeri. High-energy-resolution measurements of an ultracold-atom–ion collisional cross section. *Phys. Rev. A*, 103:032805, Mar 2021.
- [44] M. Aymar, R. Guérout, and O. Dulieu. Structure of the alkali-metal-atom strontium molecular ions: Towards photoassociation and formation of cold molecular ions. *Journal of Chemical Physics*, 135(6), 2011.
- [45] O. Katz, M. Pinkas, N. Akerman, and R. Ozeri. Quantum suppression of cold reactions far from the quantum regime. 2022. arXiv preprint arXiv:2208.07725.
- [46] M. Cetina, A. T. Grier, and V. Vuletić. Micromotion-induced limit to atom-ion sympathetic cooling in Paul traps. *Physical Review Letters*, 109(25):1–5, 2012.
- [47] T. Sikorsky, Z. Meir, R. Ben-shlomi, N. Akerman, and R. Ozeri. Spin-controlled atom–ion chemistry. *Nature Communications*, 9:920, 2018.
- [48] T. Feldker, H. FÜRST, H. Hirzler, N. V. Ewald, M. Mazzanti, D. Wiater, M. Tomza, and R. Gerritsma. Buffer gas cooling of a trapped ion to the quantum regime. *Nature Physics*, 16(4):413–416, 2020.
- [49] P. D. Gregory, M. D. Frye, J. A. Blackmore, E. M. Bridge, R. Sawant, J. M. Hutson, and S. L. Cornish. Sticky collisions of ultracold RbCs molecules. *Nature Communications*, 10, 12 2019.
- [50] C. Zipkes, L. Ratschbacher, C. Sias, and M. Kohl. Kinetics of a single trapped ion in an ultracold buffer gas. *New Journal of Physics*, 13, 2011.
- [51] K. Chen, S. T. Sullivan, and E. R Hudson. Neutral gas sympathetic cooling of an ion in a paul trap. *Physical review letters*, 112(14):143009, 2014.
- [52] M. Pinkas, Z. Meir, T. Sikorsky, R. Ben-Shlomi, N. Akerman, and R. Ozeri. Effect of ion-trap parameters on energy distributions of ultra-cold atom-ion mixtures. *New Journal of Physics*, 22(1), 2020.



# Methods

## EXPERIMENTAL SEQUENCE

A cloud of  $^{87}\text{Rb}$  atoms is trapped and cooled down using a magneto-optical trap (MOT), followed by a dark-MOT stage and a polarization gradient cooling. A cloud of  $\sim 10^6$  atoms is loaded into an optical lattice created by counter-propagating 1064 nm laser beams. The atoms are pumped into one of the hyperfine states  $|1, -1\rangle$  or  $|1, +1\rangle$  by a sequence of MW and optical pulses. The ion is Doppler cooled and subsequently cooled near its ground state with  $\bar{n} < 0.5$  in each of the motional modes. The atoms are moved to the lower chamber by changing the relative frequency between lattice beams. Unless stated otherwise, the atoms are moved over the ion in a velocity of 0.14 m/s, which is equivalent to a kinetic energy of 100  $\mu\text{K}$ . The current in the quantization coils is ramped up or down after cooling of the ion and 30 ms before the collision. Due to eddy currents in the system, the magnetic field has a transient time of 5ms. The current in the quantization coils is returned to its initial value after the collision. The detection of the spin state was done 70 ms after the collision ends and consists of two stages. First, we apply two pi pulses from the spin state that was not the initial state to two different states in the  $D_{5/2}$  manifold (double shelving). For example, in the exothermic transition, the ion is initialized at  $|+1/2\rangle$ , the detection pi pulses are  $|-1/2\rangle \rightarrow |-5/2\rangle$  and  $|-1/2\rangle \rightarrow |+3/2\rangle$ . After the shelving pulses, a fluorescence detection scheme is applied to check whether the ion spin changed or not. If spin exchange did not occur, the ion remain in the  $S_{1/2}$  manifold and will appear bright. Otherwise, it shelved into the  $D_{5/2}$  manifold and no photons are detected.

## MEASURING THE LANGEVIN COLLISIONS PROBABILITY

We measured the atomic density by measuring the failure probability to shelve the ion from the electronic ground state to the D level using a long shelving pulse (14.6  $\mu\text{s}$ ) in the presence of large EMM energy ( $E_{\text{EMM}} = 2.5 \text{ K}$ ). Under these conditions, a Langevin collision will efficiently couple the EMM energy to the secular motion [50, 51], and by that decrease the shelving probability. We numerically simulate this process [45], and find that the expected probability for a shelving failure per Langevin collision is about 87%.

We measure the shelving-failure probability per passage of the cloud and present it in Fig. 1 as the probability of observing the ion in a bright state after two shelving pulses as a function of the velocity of the ultracold atomic cloud. We find that the probability fits

well to  $p_{\text{bright}} = a/v_{\text{lattice}} + p_{\text{bg}}$  where the first term is expected from the inverse dependence of the interaction time on the lattice velocity, but the second term describes a constant background. From maximum likelihood estimation,  $\rho K_{\text{L}} = 0.039(3)$  and  $p_{\text{bg}} = 0.078(8)$ . The background probability is not due to finite shelving efficiency (98.4(3)%), but likely due to hot atoms that are not trapped in the lattice. Taking into account the detection efficiency of a collision, at a collision energy of 100  $\mu\text{K}$ , the probability for a cold Langevin collision in a single pass is  $p_{\text{L}}^{\text{lattice}}=0.32(3)$  with a background of about  $p_{\text{L}}^{\text{bg}}=0.089(4)$ . This value corresponds to the probability to have at least one collision in a pass. Assuming the number of collision in a single pass has a Poisson distribution, the mean number of collisions per pass is  $\langle N \rangle=0.385$ , with a probability of  $p_{\text{L}}^{\text{single}}=0.26$  for a single collision and  $p_{\text{L}}^{\text{multiple}}=0.06$  for multiple collisions.

## RABI CARRIER THERMOMETRY

The temperature of the ion after a collision is measured by Rabi carrier thermometry [21, 52]. The probability of observing the ion in the  $D_{5/2}$  manifold after a resonant pulse driving the  $S_{1/2} \rightarrow D_{5/2}$  transition with duration  $t$  is given by [25]

$$P_D(t) = \sum_{\mathbf{n}} P(\mathbf{n}) \sin^2(\Omega_{\mathbf{n},\mathbf{n}}), \quad (1)$$

where  $P(\mathbf{n})$  is the occupation probability of the Fock state  $\mathbf{n}$ . Here  $\Omega_{\mathbf{n},\mathbf{n}}$  the coupling strength between

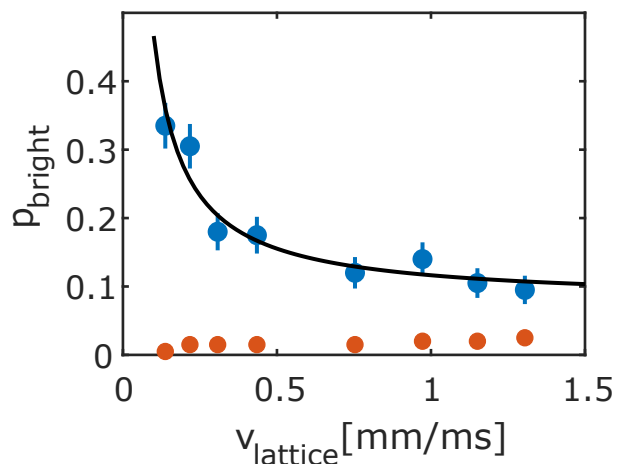


Figure 1. Calibration of the number of Langevin collisions. The probability of observing the ion in a bright state after two shelving pulses is proportional to the probability for more than one Langevin collision.

$|S_{1/2}\rangle|\mathbf{n}\rangle$  and  $|D_{5/2}\rangle|\mathbf{n}\rangle$  is given by[25]

$$\Omega_{\mathbf{n},\mathbf{n}} = \Omega_0 \prod_i e^{\eta_i^2/2} L_{n_i}(\eta_i^2),$$

where  $\Omega_0$  is the scaled interaction strength,  $\eta_i$  is the Lamb-Dicke parameter of the  $i$ -th mode, and  $L_n(x)$  is the  $n$ -th Laguerre polynomial. The Fock states are assumed to be distributed thermally with a mean occupation number  $\bar{\mathbf{n}}$ ,

$$P(\mathbf{n}; \bar{\mathbf{n}}) = \prod_i \frac{1}{\bar{n}_i + 1} \left( \frac{\bar{n}_i}{\bar{n}_i + 1} \right)^{n_i}.$$

At higher temperatures, more values of  $n$  need to be considered in this distribution. At temperature above 2 mK, we approximate the energy distribution by

$$P(E) = \frac{1}{(k_B T)^3} E^2 e^{-\frac{E}{k_B T}}$$

where  $E = \sum_i \hbar \omega_i n_i$  and  $n_i$  is taken over a logarithmic scale. The contrast of a Rabi cycle post-selecting the spin-state proportional to the spin-exchange probability is given by

$$P_D(t; p_{SE}) = p_{SE}^{\text{pass}} P_D(t).$$

The parameters  $T$ ,  $\Omega_0$  and  $p_{SE}^{\text{pass}}$  are found by maximum-likelihood estimation of the experimental results to  $P_D(t; p_{SE})$  assuming that the number of dark events follows a binomial distribution.

### AVOIDED-CROSSING DUE TO TRAPPING RF FIELD

Due to the oscillating electric field, there is an oscillating magnetic field on the ion with the same frequency, 26.5 MHz. This creates an avoided crossing when the Zeeman gap in the ground state of the ion is equal to this frequency, at 9.5 G. As a result, if the ion is prepared in  $|\downarrow\rangle$  and the magnetic field during the collision is above this threshold, the collision will occur when the ion is in the  $|\uparrow\rangle$ , and similarly for the opposite state. Therefore, for measurements above this threshold with ion in  $|\uparrow\rangle$ , the ion should be prepared in the  $|\downarrow\rangle$  state, and vice versa.

### AMPLIFICATION OF INELASTIC PROCESSES

We can build a simple probabilistic model that relate the number of short-range collisions and the short-range spin-exchange (SE) probability to the amplification of the exothermic SE probability as a function of the magnetic field. Assume that a bound state consists of  $n$

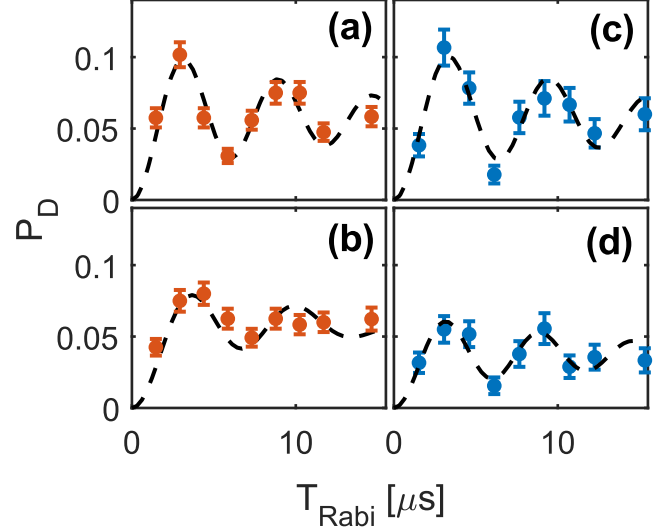


Figure 2. Rabi carrier thermometry after post-selecting SE events. (a-b) exothermic transitions at 3 G (a) and 20 G (b). (c-d) endothermic transitions at 3 G (c) and 20 G (d). Temperatures and contrast of the Rabi oscillation are written in Table I

short-range collisions, where  $n$  has a geometric distribution with a probability  $p = 1/\langle N \rangle$ . For each short-range collision, the SE probability,  $p_{SE}^0$ , is constant.

If there is no magnetic field, the short-range SE events are independent. Therefore, for a given  $n$ , the number of SE events,  $n_{SE}$ , has a binomial distribution. In the experiment, only odd number of SE events are detected, and therefore the effective measured SE probability is given by

$$p_{SE}^{\text{eff}}(B=0) = \sum_{n=1}^{\infty} (1-p)^{n-1} p \sum_{n_{SE} \text{ odd}}^n B(n_{SE}; n, p_{SE}^0),$$

where

$$B(n_{SE}; n, p_{SE}^0) = \binom{n}{n_{SE}} (p_{SE}^0)^{n_{SE}} (1-p_{SE}^0)^{n-n_{SE}},$$

is the binomial distribution. On the other hand, if the magnetic field is larger than the binding energy, only one exothermic SE event is allowed. In this case the effective probability is

$$p_{SE}^{\text{eff}}(B \rightarrow \infty) = \sum_{n=1}^{\infty} (1-p)^{n-1} p \sum_{m=1}^n (1-p_{SE}^0)^{m-1} p_{SE}^0$$

Then, we can calculate the the ratio  $p_{SE}^{\text{eff}}(B=0)/p_{SE}^{\text{eff}}(B \rightarrow \infty)$  for any  $N$  and  $p$ , as shown in Fig. 3. From the probability of exothermic SE as function of the magnetic field (in Fig. 3) we can find the ratio

Channel	B [G]	T (atoms) [mK]	Contrast (atoms)	T (bg) [mK]	Contrast (bg)
Exothermic	3	1.3(5)	11.4(4)	0.24(3)	0.98(2)
Exothermic	20	4.4(4)	12.3(5)	0.41(5)	0.97(2)
Endothermic	3	1.2(2)	11.4(6)	0.21(2)	0.99(2)
Endothermic	20	1.5(4)	7.4(5)	0.24(4)	0.96(2)

Table I. Temperatures and contrasts fitted to Rabi cycles for different spin-exchange channels with the corresponding temperature and contrast measured on the same transition without atoms.

$p_{SE}^{\text{eff}}(B=0)/p_{SE}^{\text{eff}}(B \rightarrow \infty)$ , as shown in the red shaded region in Fig. 3. On the other hand, the short-range SE probability was found in the fit to the exothermic data in Fig. 2, denoted by the blue line. From crossing these two curves, we can estimate the mean number of short-range collisions,  $\langle N \rangle = 10(3)$ .

### MOLECULAR DYNAMICS SIMULATION

We numerically solve the classical equations of motion that cast by the atom-ion Hamiltonian

$$\hat{H} = \frac{\hat{p}_i^2}{2m_i} + \frac{\hat{p}_a^2}{2m_a} + V(|\hat{r}_i - \hat{r}_a|) + \frac{1}{2}m_i\omega^2\hat{r}_i^2, \quad (2)$$

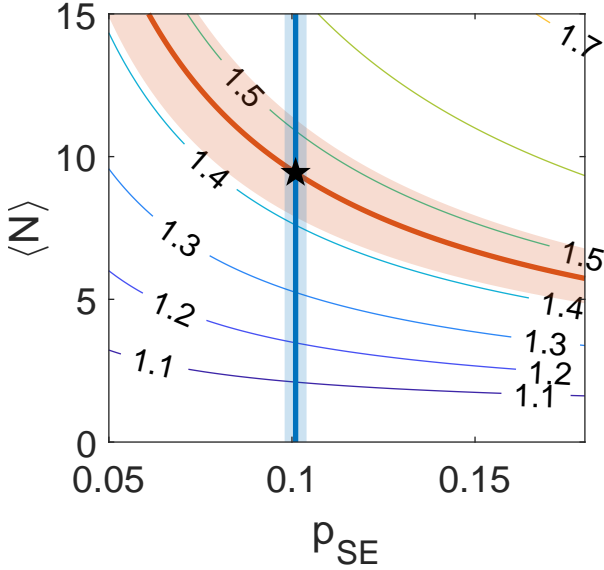


Figure 3. Ratio of the exothermic SE probability at high magnetic field ( $p_{SE}(B=0)$ ) to SE probability at zero magnetic field ( $p_{SE}(B \rightarrow \infty)$ ) as function of the short-range SE probability,  $p_{SE}$ , and the mean number of short-range collisions,  $\langle N \rangle$ . This ratio is calculated from a model for a bound state. Red and blue bold lines are the measured ratio and short-range SE probability, respectively, with  $1\sigma$  confidence bound in shaded area. The star is the crossing of these curves, indicating the mean number of short-range collisions,  $\langle N \rangle^{exp} = 10(3)$ .

where  $m_{i(a)}$  is the ion (atom) mass,  $\hat{r}_{i(a)}$  is the ion (atom) position,  $\hat{p}_{i(a)}$  is the ion (atom) momentum,  $\omega$  is the secular frequency of the spherical ion trap and  $V(\hat{r}_i - \hat{r}_a)$  is the atom-ion interaction potential. We use the asymptotic form of the atom-ion interaction potential  $V(r) = -2C_4/|\hat{r}_i - \hat{r}_a|^4$  at all distances larger than 10 nm, where the coefficient  $C_4 = 1.05 \cdot 10^{-56} \text{ J}\cdot\text{m}^4$  is determined predominantly by the neutral atom polarizability. The short-range atom-ion potential is modeled by an infinite wall at 10 nm. At this point, the particles collide in an elastic hard-sphere collision. Without spin-exchange, after the collisions the velocities in the collision axis are changed assuming conservation of momentum and energy in the center of mass frame. Because the masses of  $^{87}\text{Rb}$  and  $^{88}\text{Sr}^+$  are nearly equal, the velocities are as well nearly equal but change their sign in the center of mass frame.

Based on Refs. [33, 46, 52] the trajectories of the atom and ion are governed by Newton's equations of motion. The Atoms start their trajectory on a plane  $1.2 \mu\text{m}$  from the center of the trap and the ion have an initial temperature of  $150 \mu\text{K}$  (unless stated otherwise) divided equally in the different secular motional modes. The velocity distribution of the atoms consists of two terms, a thermal term ( $T = 5 \mu\text{K}$ ) and a constant velocity which corresponds to the velocity of the optical lattice.

The kinetic effect of a spin exchange process is modeled by energy absorption or release after the hard-sphere collision. The probability of a SE to happen is calculated by acceptance-rejection method, for the given  $p_{SE}^0$  value. If spin-exchange occurred, the momentum and energy is no longer conserved. The momentum is altered only along the collision axis, and the ion and atoms velocities parallel to the collision axis after the collision are updated by

$$u_i^{\parallel} = v_{cm}^{\parallel} + \frac{1}{m_i} \sqrt{\frac{2\Delta E}{\mu} + \left(\frac{|v_i - v_a|}{\mu}\right)^2},$$

$$u_a^{\parallel} = v_{cm}^{\parallel} - \frac{1}{m_a} \sqrt{\frac{2\Delta E}{\mu} + \left(\frac{|v_i - v_a|}{\mu}\right)^2}.$$

where  $\Delta E = hB \cdot 3.5 \text{ MHz}$ ,  $h$  is Planck constant,  $v_{cm}^{\parallel}$  in the center-of-mass velocity parallel to the collision axis, and  $3.5 \text{ MHz/G}$  is the Zeeman energy gap in a spin-exchange transition when the ion and the atom are in

the electronic ground state.

### Calculating effective SE in the presence of EMM

An excess micromotion is induced by a constant field, and can be introduced into the simulation by an additional acceleration term,

$$\ddot{\mathbf{x}} = \frac{e\mathbf{E}^{\text{dc}}}{m_i} \quad (3)$$

where  $e$  is the electron charge. Only radial EMM is assumed, divided equally between the radial modes. For a total EMM energy  $E_{\text{EMM}}$ , the electric field in the  $j$ -th mode direction is,

$$E_j^{\text{dc}} = 2\sqrt{\frac{2E_{\text{EMM}}}{m_i\Omega^2}} \frac{m_i\omega_j^2}{q_j e}. \quad (4)$$

We can calculate numerically the probability density function,  $p(n; E_{\text{EMM}})$ , for  $n$  short-range collisions, when the total EMM energy is  $E_{\text{EMM}}$ . In the case of exothermic transition in the presence of large enough magnetic field, we can assume a spin-exchange event happens at most one time. The effective SE probability per Langevin collision is given by

$$p_{\text{SE}}^{\text{eff}}(E_{\text{EMM}}; p_{\text{SE}}^0) = \sum_{n=1}^{\infty} p(n; E_{\text{EMM}}) \sum_{m=1}^n (1-p_{\text{SE}}^0)^{m-1} p_{\text{SE}}^0. \quad (5)$$

For a given  $p_{\text{SE}}^0$  we can calculate  $p_{\text{SE}}^{\text{eff}}(E_{\text{EMM}}; p_{\text{SE}}^0)$ . Since the probability for a collision in a single passage,  $p_{\text{L}}^{\text{lattice}}$ , is less than one, and there are contributions from hot collisions with probability  $p_{\text{L}}^{\text{bg}}$ , the effective observed probability from the simulation is given by

$$p_{\text{SE}}^{\text{pass}}(E_{\text{EMM}}; p_{\text{SE}}^0) = p_{\text{L}}^{\text{lattice}} p_{\text{SE}}^{\text{eff}} + p_{\text{L}}^{\text{bg}} p_{\text{SE}}^0. \quad (6)$$

Using maximum likelihood estimation, we find the  $p_{\text{SE}}^0$  that maximize the likelihood function.

Although the EMM is compensated throughout the experiment, the measured data is not center around the zero voltage on the compensation electrode. Therefore, the center of the curve was found before finding the short-range  $p_{\text{SE}}^0$ . The center was found by a parabola fit to  $p_{\text{SE}}^{\text{pass}}$  as function of  $\Delta V_{\text{comp}}$ . The center is shifted by 0.2073 V on the compensation electrode, corresponds to 40  $\mu\text{K}$ .